Inner-Shell Excitation Spectroscopy of Fused-Ring Aromatic Molecules by Electron Energy Loss and X-ray Raman Techniques

Michelle L. Gordon,[†] David Tulumello,[†] Glyn Cooper,[†] Adam P. Hitchcock,*[,†] Pieter Glatzel,[‡] Oliver C. Mullins,[§] Stephen P. Cramer,[||,⊥] and Uwe Bergmann[||,⊥]

Department of Chemistry, McMaster University, Hamilton, ON, L8S 4M1, Canada, Department of Chemistry, Utrecht University, 3584 CA Utrecht, The Netherlands, Schlumberger-Doll Research, Ridgefield, Connecticut 06877, Department of Applied Science, University of California, Davis, California 95616, and Physical Biosciences Division, Lawrence Berkeley National Laboratory, Berkeley, California 94720

Received: June 6, 2003; In Final Form: August 6, 2003

Oscillator strengths for C 1s excitation spectra of gaseous benzene, naphthalene, anthracene, phenanthracene, triphenylene, pyrene, and 1,2-benzanthracene have been derived from inner-shell electron energy loss spectroscopy recorded under scattering conditions where electric dipole transitions dominate (2.5 keV residual energy, $\theta \leq 2°$ corresponding to a product of momentum transfer and C 1s orbital size (qr) of 0.08). These spectra are interpreted with the aid of ab initio calculations on selected species. They are compared to the C 1s spectra of solid samples of benzene, naphththalene, anthracene, triphenylene, and 1,2-benzanthracene, recorded with inelastic X-ray Raman scattering in the dipole limit ($qr < 0.5$). When differences in resolution are taken into account, good agreement is found between the inelastic electron scattering spectra of the gases and the inelastic photon scattering spectra of the corresponding solid. Small differences are attributed to quenching of transitions to Rydberg states in the solids. Characteristic differences related to the degree of symmetry or spatial arrangement of the fused ring aromatic hydrocarbons (e.g., linear versus bent structures) indicate that C 1s X-ray Raman spectroscopy should be useful for characterizing aromatics in bulk samples that are opaque to soft X-rays, such as coals and heavy hydrocarbon deposits.

1. Introduction

Fused aromatic compounds are important species in heavy hydrocarbon and coal chemistry.[1] Techniques to characterize the aromatic hydrocarbon species present are of interest with regard to improved methods of recovery and to understand morphogenesis of these materials. Methods that break up the structure of hydrocarbon materials and extract the aromatic components are used, but there are some concerns that the extraction chemistry could modify the distribution of species present. Ideally one would like techniques that could be applied without modifying the hydrocarbon material. Inelastic X-ray Raman scattering (XRS)[2] is a promising technique in this regard since 6−10 keV X-rays can readily penetrate appreciable thicknesses of these materials. High-intensity synchrotron radiation and recent instrumental advances[3] have made this technique practical, and first studies of asphaltene have been performed.[4,5]

To study complex mixtures of aromatic species, it is important to have reliable spectra of the pure components and to understand the links between geometric/electronic structure and the observed spectra. In addition, since there is appreciable momentum transfer in the XRS experiment, questions arise as to the possible contributions of nondipole transitions. For these reasons we have carried out a comparative study of a number of fused aromatics by XRS of the solid and by inelastic electron scattering (also called inner-shell electron energy loss spectroscopy (ISEELS)[6,7]) of the gaseous species. ISEELS has been used under small momentum transfer conditions to study a large number of gas phase species.[8] Under these conditions electric dipole transitions dominate. Thus, any deviations between ISEELS and XRS spectra are evidence for either a difference in the spectroscopy between gas and solid phases or possibly nondipole contributions to XRS on account of the finite momentum transfer. Of the species investigated in this work, benzene has been studied extensively by both ISEELS[9,10] and NEXAFS.[11−13] The C 1s ISEELS spectrum of naphthalene has been reported and interpreted with the aid of extended Hückel calculations in the equivalent cores (Z+1) approximation.[14]

This paper is organized as follows: Section 2 describes the experimental procedures for ISEELS and XRS, as well as the GSCF3 computations used for selected species. Section 3 reports the ISEELS and XRS spectra, their comparison, and the interpretation aided by computational results on naphthalene, anthracene, and triphenylene, and section 4 summarizes the results.

2. Experimental Section

2.1. Electron Energy Loss Spectroscopy. All samples were obtained from Sigma Aldrich in the form of crystalline powders and had a stated purity better than 99%. They were used without further purification. Except for benzene, to get adequate vapor pressure at the collision site, the samples were placed inside a small aluminum tube attached directly to the collision cell of the spectrometer. In all cases except naphthalene the collision cell was heated to 80−150 °C using an internally mounted quartz-halogen bulb. The end plates of the collision cell were

[†] McMaster University.
[‡] Utrecht University.
[§] Schlumberger-Doll Research.
[||] University of California.
[⊥] Lawrence Berkeley National Laboratory.

10.1021/jp035607r CCC: $25.00
Published on Web 09/23/2003

TABLE 1: Geometries (all planar ($z = 0$)) and Basis Sets for Core Excitation GSCF3 Computations

	coordinates (Å)			coordinates (Å)	
	x	*y*		*x*	*y*
Naphthalene			Triphenylene		
C	0.000	0.707	C	−2.440	0.707
C	−1.210	1.401	C	−2.440	−0.707
C	−2.420	0.707	C	−1.220	−1.414
C	−2.420	−0.707	C	0.000	−0.707
C	−1.210	−1.401	C	0.000	0.707
C	0.000	−0.707	C	−1.220	1.414
C	1.210	−1.401	C	1.220	−1.414
C	2.420	−0.707	C	2.440	−0.707
C	2.420	0.707	C	2.440	0.707
C	1.210	1.401	C	1.220	1.414
H	−1.210	2.540	C	3.660	1.414
H	−3.380	1.262	C	3.660	2.828
H	−3.380	−1.262	C	2.440	3.535
H	−1.210	−2.540	C	1.220	2.828
H	1.210	−2.540	C	1.220	−2.828
H	3.380	−1.262	C	2.440	−3.535
H	3.380	1.262	C	3.660	−2.828
H	1.210	2.540	C	3.660	−1.414
Anthracene			H	−1.220	2.514
C	−3.60	0.72	H	−3.393	1.207
C	−2.41	1.39	H	−3.393	−1.207
C	−1.22	0.72	H	−1.220	−2.514
C	0.00	1.39	H	0.267	−3.378
C	1.22	0.72	H	2.440	−4.635
C	2.43	1.39	H	4.613	−3.378
C	3.64	0.72	H	4.613	−0.864
C	3.60	−0.72	H	4.613	0.864
C	2.41	−1.39	H	4.613	3.378
C	1.22	−0.72	H	2.440	4.635
C	0.00	−1.39	H	0.267	3.378
C	−1.22	−0.72			
C	−2.43	−1.39			
C	−3.64	−0.72			
H	−4.56	1.27			
H	−2.41	2.49			
H	0.00	2.49			
H	2.41	2.49			
H	4.56	1.27			
H	4.56	−1.27			
H	2.41	−2.49			
H	0.00	−2.49			
H	−2.41	−2.49			
H	−4.56	−1.27			

Naphthalene Basis Set: (Huzinaga contracted Gaussian type orbitals)

HTS8X 7	411121 21111	for core hole
PGM6G	xxx	2* d-polarization (xxx = element specific) on core hole
HTS6X 6	63 5	for noncore hole C
HTS3X 1	6	for H

Anthracene and Triphenylene Basis Sets: (Huzinaga contracted Gaussian type orbitals)

HTS6X 7	41121 2111	for core hole
PGM6G	xxx	2* d-polarization (xxx = element specific) on core hole
HTS4X 6	53 4	for noncore hole C
HTS3X 1	6	for H

water cooled to trap the vaporized sample and to avoid depositing insulating material on sensitive parts of the spectrometer. Multiple spectra were recorded to confirm reproducibility and to check for possible thermal decomposition of the samples.

C 1s electron energy loss spectra were acquired with a gas phase ISEELS spectrometer operated with a small scattering angle (∼2°) and a high electron impact energy (2.5 keV + energy loss), corresponding to a momentum transfer (q) of 0.94 Å^{-1}. The spectrometer resolution is dependent on the electron beam current and analyzer pass energy, but is typically 0.75 eV full width at half-maximum (fwhm) at a beam current of 20 μA and 0.50 eV fwhm for a beam current of ∼1 μA. The reported spectra are combinations of low-current spectra recorded in the region of the sharp structure (284−296 eV) and high current spectra recorded outside this region. Care was taken to match the signals at the joined regions. The energy scales of all spectra were calibrated by acquiring the spectra of a stable mixture of the analyte molecule and a reference compound. The C 1s and O 1s spectra of both molecules were calibrated using the C 1s → π^* (290.74(4) eV) and the O 1s → π^* (535.4 (2) eV) transitions of CO_2.[15] The C 1s signals were isolated from the underlying valence-shell ionization continua by subtracting a smooth curve determined from a curve fit of the function $a(E - b)^c$ to the pre-edge experimental signal. The background subtracted spectra are converted to absolute oscillator strength scales using previously described methods.[8]

2.2. X-ray Raman Scattering. Samples were acquired from

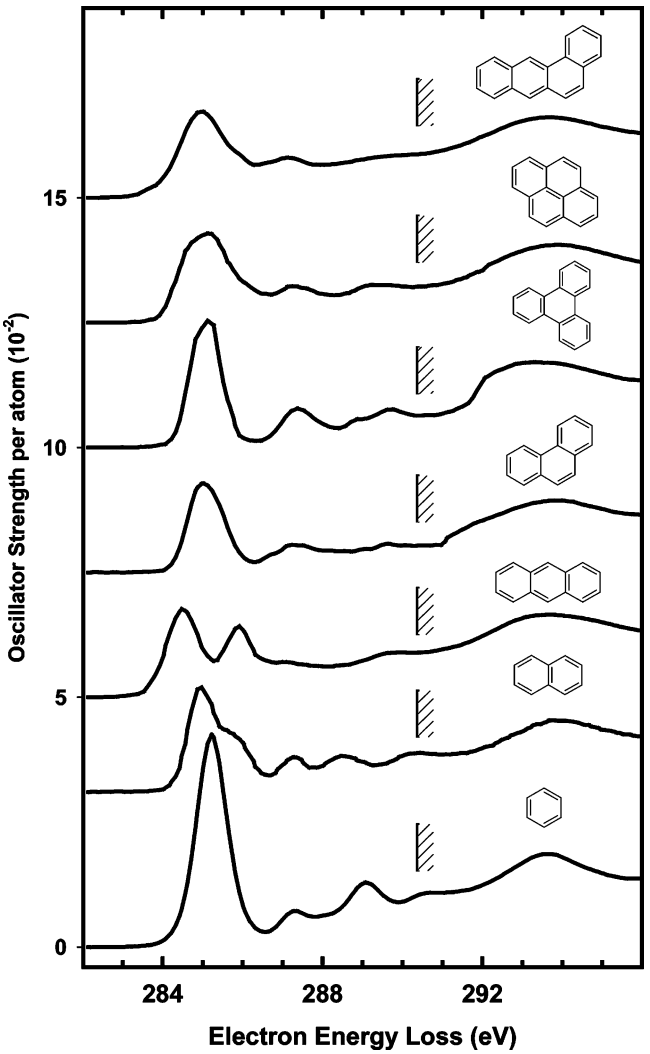

Figure 1. C 1s oscillator strength spectra of benzene, naphthalene, anthracene, phenanthracene, triphenylene, pyrene, and 1,2-benzanthracene. All of the spectra were derived from energy loss spectra recorded under near-dipole scattering conditions (2500 eV impact energy, 2° scattering angle) with 0.55 eV fwhm resolution. The hatched lines indicate the C 1s IPs as determined by X-ray photoelectron spectroscopy or estimated from XPS of similar species.[28]

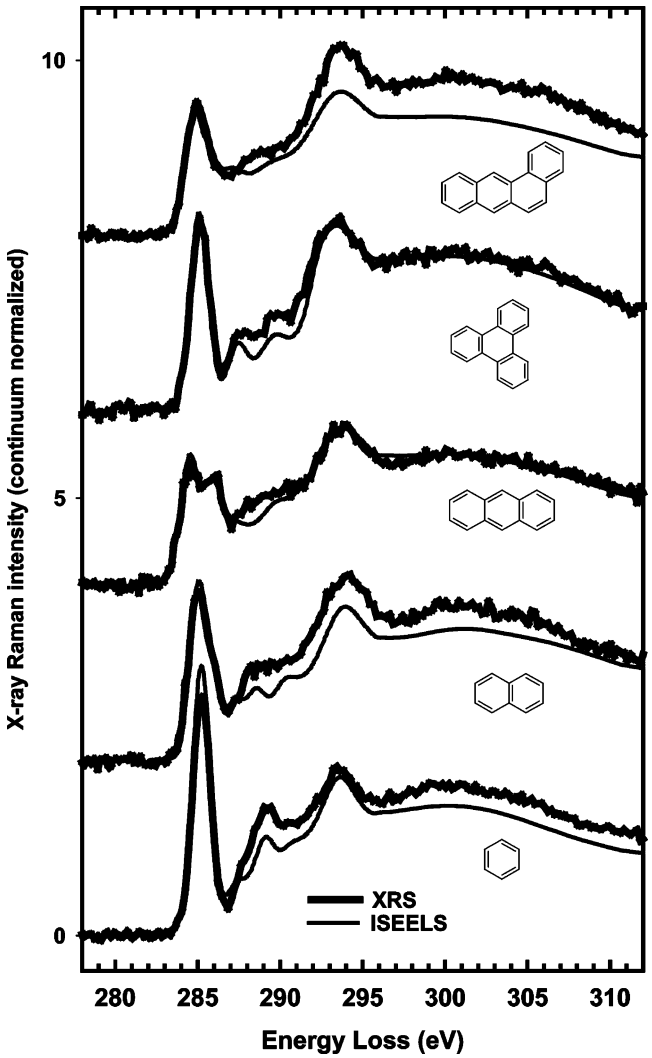

Figure 2. (thick lines) C 1s inelastic X-ray scattering spectra of benzene, naphththalene, anthracene, triphenylene, and 1,2-benzanthracene. (thin lines) ISEELS spectra of the same species, broadened by smoothing to match the width of the lowest energy π^* band. Offsets are used for clarity.

Aldrich Chemical Co. and used without further purification. Except for benzene, all samples were pressed into ~5 × 5 mm cylindrical pellets and were run at room temperature. Benzene was frozen in liquid nitrogen and measured in a He flow through a cryostat operated at ~10 K.

The XRS measurements were performed at the BioCAT undulator beamline 18ID at the Advanced Photon Source. A cryogenically cooled Si(1,1,1) monochromator operated at an

TABLE 2: Energies (eV) and Proposed Assignments for Features in the C 1s Spectrum of Gaseous Benzene (Bz), Napththalene (Na), Anthracene (An), Phenanthracene (Pa), Triphenylene (Tp), Pyrene (Py), and 1,2-Benzanthracene (Ba) Recorded by ISEELS

	energy (±0.1 eV)							
no.	Bz	Na	An	Pa	Tp	Py	Ba	assignment (final orbital)
1	285.2[a]	285.0[a]	284.5[a]	285.1[a]	284.8	284.7	283.7 (sh)	1π^*
2		285.7	285.9		285.1[a]	285.1[a]	285.0[a]	1π^*
3 (sh)		286.9		286.7		285.9	285.8	
4	287.2	287.2						3s
5			287.0	287.3	287.4	287.3	287.1	3s, 1π^* or 2π^*
6	289.1	288.5		288.3	288.9	289.1		3p, 2π^*, σ^*(C−H)
7				289.1	289.8	289.7		3p, 2π^*, σ^*(C−H)
8	290.6	290.3	289.7	289.6			289.6	2π^*, σ^*(C−H), higher Rydbergs
IP								
9	293.5	293.9	293.7	293.8	293.4	293.8	293.6	2π^*, σ^*(C−H), 2e$^-$
10	299.2	300.6	300.5	300.5	298.3	299.6	300.2	σ^*(C−C)
11	301.9				301.5			σ^*(C−C)
12		306.0	305.6	306.1	306.0	306.2	305.6	σ^*(C−C)

[a] Calibration: Bz (5.54(4)) relative to CO_2 π^* (290.74 eV); Na (2.46(4)); An (2.89(2)); Pa (2.32(3)); Tp (2.33(3)); Py (2.35(3)); Ba (2.43(2)) relative to CO π^* (287.40 eV).

TABLE 3: Energies (eV) and Proposed Assignments for Features in the C 1s Spectrum of Solid Benzene (Bz), Napththalene (Na), Anthracene (An), Triphenylene (Tp), and 1,2-Benzanthracene (Ba) Recorded by X-ray Raman Scattering

	energy (±0.1 eV)					
feature	Bz	Na	An	Tp	Ba	assignment (final orbital)
1	285.2[a]	285.0[a]	284.6[a]	285.1[a]	284.9[a]	1π*
2		285.9	285.9		285.6	1π*
4	287.8					3s
5				287.5		3s, 1π* or 2π*
6	289.2	288.1	288.0	288.8		3p, σ*(C−H), 2π*
7			288.7	289.5	288.5	2π*,σ*(C−H)
8	290.6	(290.3)	(290.2)			2π*, σ*(C−H), higher Rydbergs converging to IP(s)
IP						
9	293.5	294.2	293.6	293.4	293.8	2π*, σ*(C−H), 2e-
10	299.3	300.6	300.3	300.9	300.2	σ*(C−C)
12	303.5	305.3	305.3		306.0	σ*(C−C)

[a] Calibration: Bz (0.17); Na (0.37); An (0.77); Tp (0.27); Ba (−0.47) relative to graphite π* (285.37[30]).

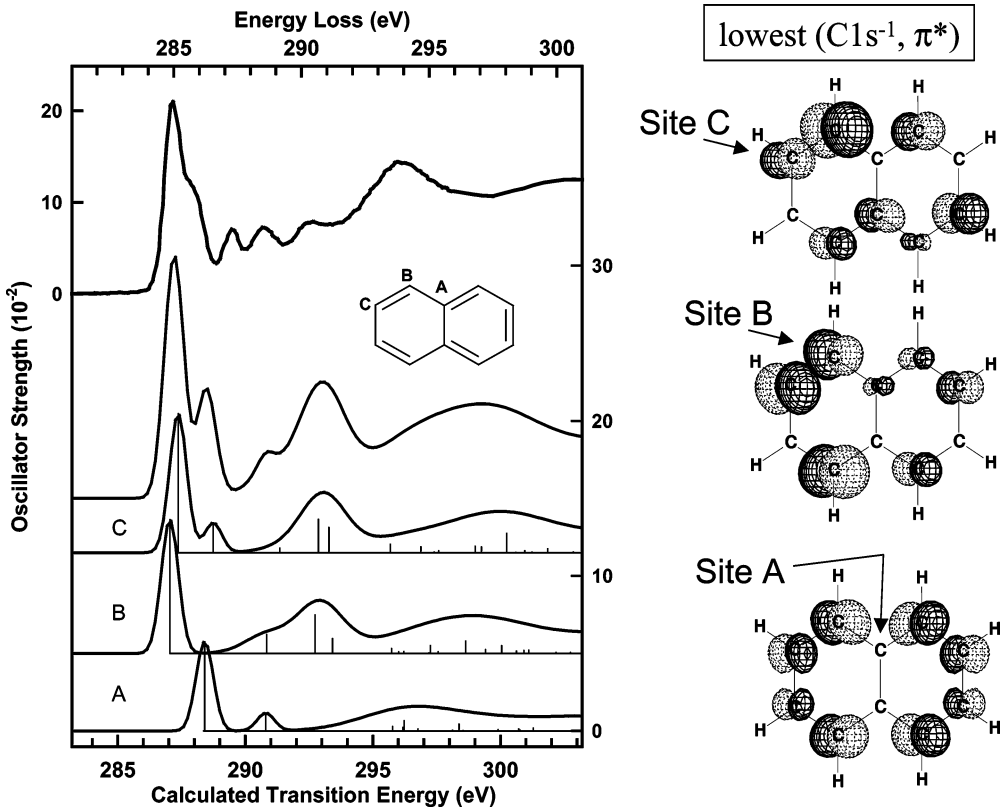

Figure 3. Computed versus measured (ISEELS) spectra of naphthalene. The calculated spectrum for each site is shown, along with the spectral components and the weighted sum. The MO plots show the LUMO with a localized core hole at the indicated site. Note that this approach breaks the molecular symmetry, and thus the true representation of the LUMO would be one that is the superposition of MOs with the core hole at each symmetry equivalent site.

energy of 6760 ± 50 eV was used for the incident beam. A high-resolution multicrystal spectrometer was used to analyze the Raman scattered radiation. The instrument is based on spherically curved Johann type crystals aligned on intersecting Rowland circles. Eight 3.5 in. diameter Si(4,4,0) crystals, each with a radius of curvature of 86 cm, were operated at a Bragg angle of 87°. The total energy resolution, given by the convolution of monochromator and analyzer resolution, was determined to be 1.1 eV fwhm by measuring the quasi-elastic scattering at 6466 eV. The incident flux was on the order of 3×10^{13} photons/s with a beam size $\sim 0.2 \times 1$ mm^2. To avoid radiation damage, the beamline monochromator was operated in continuous scanning mode, where the sample was automatically repositioned to a fresh spot after each scan, which took 140 s. Between 5 and 20 of such scans were averaged per sample spectrum. Baseline subtraction was done by fitting an empirical formula of the type $y = a(E - b)^c$ (a,b,c are free fit parameters) to the pre-edge region. It turned out that variation of c did not significantly affect the fit result, and c was then fixed to -1.

As a consequence of the geometry of the multicrystal analyzer array, the Raman scattering angles spanned a range from 70° to 129°, resulting in momentum transfers, $3.84 < q < 6.06$ Å^{-1}. Estimates of the dipole condition of XRS based on both the orbital radius[16,17] and the orbital diameter[18] have been reported in the literature. Using the carbon 1s orbital radius $r \approx a_0/Z = 0.088$ Å leads to $0.34 < qr < 0.53$. This number lies within the dipole approximation, whereas the same estimate using the orbital diameter would no longer be in the accepted range for validity of the dipole approximation ($qr < 0.5$). Recently there has been a study that shows nondipole contributions in, for example, LiF at similar q values.[19] However the orbital radius of Li is approximately twice as large as that of carbon, leading

TABLE 4: Selected Eigenvalues, Oscillator Strengths, and Orbital Characters for Computed Core-Excited States of Naphthalene

site	IP	character (symmetry)[a]	orbital	$-\epsilon$ (eV)	$f(10^{-2})$	$(R - Å)$
A	292.97	π^* $2b_{2g}$	35	−4.578	0.00	2.315
		π^* $2b_{3g}$	36	−4.495	2.42	2.233
		π^* $3b_{1u}$	37	−2.106	0.51	2.122
		π^* $2a_u$	38	1.227	0.00	2.541
		σ^*(C−H)	41	2.900	0.53	2.702
		σ^*(C−H)	40	3.234	0.48	2.497
		σ^*(C−H)	39	3.742	0.31	2.815
		π^* $3b_{3g}$	47	3.837	1.77	2.125
		σ^*(C−C)	45	5.437	0.87	2.698
B	292.32	π^* $2b_{2g}$	35	−5.240	1.83	2.331
		π^* $2b_{3g}$	36	−3.154	0.00	2.293
		π^* $3b_{1u}$	37	−1.447	0.64	2.106
		π^* $2a_u$	38	1.198	0.45	2.509
		σ^*(C−H)(local)	41	1.393	1.68	2.991
		σ^*(C−H)	39	3.907	0.14	3.016
		σ^*(C−H)	40	4.372	0.24	3.016
		π^* $3b_{3g}$	44	4.870	1.77	2.124
		σ^*(C−C)	47	5.211	0.06	2.698
C	292.33	π^* $2b_{2g}$	35	−4.920	1.90	2.269
		π^* $2b_{3g}$	36	−3.560	0.41	2.323
		π^* $3b_{1u}$	37	−0.925	0.15	2.064
		π^* $2a_u$	38	1.021	0.80	2.460
		σ^*(C−H)(local)	41	1.503	1.41	3.509
		σ^*(C−H)	40	4.473	0.36	2.823
		σ^*(C−H)	39	4.516	0.07	3.125
		π^* $3b_{3g}$	44	5.251	0.64	2.168
		σ^*(C−C)	51	5.797	0.76	3.193

[a] Orbital symmetry in D_{2h}, derived from matching patterns of core-excited symmetry-broken orbitals with correct symmetry, ground state orbitals. Linear combinations of localized core hole solutions would have these indicated symmetries. The designation "local" for two of the C−H σ^* assignments means that the final orbital density is localized at the C−H bond where the C 1s core hole has been created.

to *qr* values twice as large. Thus we expect only very small if any nondipole contributions in the spectra reported here. For comparison, the *qr* product for the ISEELS setup is 0.08 (*r* as radius), well within this measure of the dipole limit.

2.3. Computational Methods. To gain insight into how the inner-shell spectra reflect the electronic structure of these molecules, calculations were performed using GSCF3 (Gaussian self consistent field version 3),[20,21] which is an ab initio code designed specifically for inner-shell excitation and ionization calculations. The program uses the Hartree−Fock-SCF approach to solve for the energies and molecular orbitals of the system under investigation. The basis sets used are those of Huzinaga et al.[22] The improved virtual orbital (IVO) method,[21] which explicitly takes into account the core hole in the Hartree−Fock approximation, is used to perform quantum calculations on core-excited molecules. In this approach, the core electron is removed directly from an inner-shell orbital specified by the user. The virtual orbitals of this system provide a good approximation to the term values of the core excitation features at that site.[21] A separate calculation is performed for each distinct chemical site in each molecule (the site labeling is indicated in the figures reporting the computational results).

Table 1 lists the geometries of the molecules studied and the basis sets employed. The calculation is performed in three steps. In step one, the eigenvectors (MOs) and eigenvalues of the ground state are calculated, and the core MO that will lose the electron is determined. In the second step, the core ion state is computed by removing the user-specified core electron and allowing the system to relax and reorganize in the presence of the core hole. The difference in the total energy of the core-ionized and ground state gives the core level ionization potential (IP) with a typical accuracy of 1 eV. The third step determines the core excitation energies and transition probabilities in terms of the IVO approximation.[21] The absolute accuracy of the computed core excitation energies depends on the size of the basis set used. However, the core state term values (TV = IP − *E*) are more accurate and relatively independent of basis set choices. The core excitation term values and optical oscillator strengths generated by the third step of the GSCF3 calculation are used to generate simulated core excitation spectra by summing Gaussian lines at an energy given by the term value, an area given by the oscillator strength for excitation to each improved virtual orbital, and a width chosen as a function of the term value. In the discrete region, the chosen line width is that of the instrument. Larger line widths are used for the core states above the IP which correspond to lifetime broadened continuum resonances. The widths used are summarized in footnotes to the tables which summarize the computational results. In comparing the computed spectra to experiment, the calculated transition energies are retained but a rigid shift of the computed and experimental energy scales is built into the plot presentation. The shifts, which range from 0.6 to 3.3 eV, are typical of the inaccuracies found in other applications of GSCF3 to core excitation.

3. Results and Discussion

3.1. C 1s ISEELS Spectroscopy. Figure 1 compares the C 1s oscillator strength spectra of gaseous benzene, naphthalene, anthracene, phenanthracene, triphenylene, pyrene, and 1,2-benzanthracene derived from the inelastic electron scattering spectra. The intensity scale for each spectrum reflects the oscillator strength per carbon atom and is thus an average over the different environments in each species. The spectra were recorded over much longer energy ranges (275−350 eV), but only the 282−296 eV region is shown to allow clear view of the near edge fine structure. The spectra over the full range are available from an on-line database.[23] The energies, term values, and tentative assignments are listed in Table 2.

3.2. X-ray Raman Spectroscopy. Figure 2 presents the inelastic X-ray Raman scattering (XRS) spectra of solid benzene, naphthalene, anthracene, triphenylene, and 1,2-benzanthracene, recorded using 9 keV photon impact. The pre-C 1s signal was extrapolated and subtracted, and then the C 1s edge jump set to unity. Table 3 summarizes the energies and tentative assignments of the XRS signals. The peak numbering schemes in Tables 3 and 2 are chosen so as to align peaks at similar energies, which are assumed to have a similar origin in the gas and solid species. In addition to the XRS data, Figure 2 also plots as thin solid lines the corresponding ISEELS spectrum (converted to optical scale), after a smoothing procedure for which the parameters were adjusted so that the width of the first π^* transition matches that in the XRS spectrum. For all species, very similar smoothing parameters were used. While some fine scale features differ between the XRS and ISEELS spectra (these are discussed in detail below), overall there is remarkably good agreement, indicating that the XRS technique is recovering the dipole core excitation spectrum to a very good approximation.

3.3. Comparison of XRS and ISEELS Spectra. While the main features for each species are observed at similar locations and with similar relative intensities, there are some differences between the results of the two techniques. One of the most striking is the absence of specific peaks, as well as reduced intensity or redistributed intensity in the 287−290 eV region.

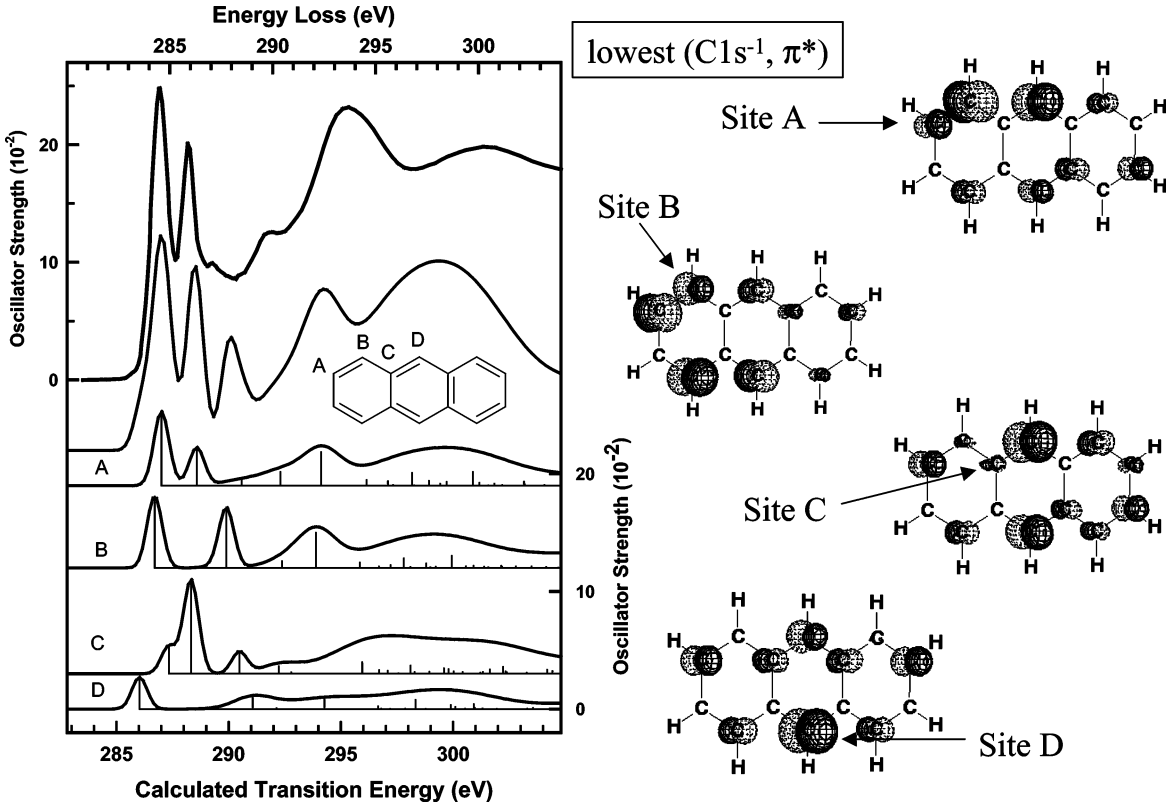

Figure 4. Computed versus measured (ISEELS) spectra of anthracene. See caption to Figure 3 for further details.

Both higher level C 1s → π^* and Rydberg transitions are expected in this region. One of the expected effects when comparing gas and solid spectra is a quenching of Rydberg transitions in the condensed state[24] and/or conversion of these transitions into excitonic states.[25] The absence, or possibly a shift to higher energy, in the XRS spectra of the solid species of the ~287 eV peaks, assigned to C 1s → 3s Rydberg transitions in the gaseous species, provides confirmation of that spectral assignment. Perhaps of more interest are the cases where the intensity is unchanged in this region since this likely indicates a significant virtual valence character to the upper level, consistent with higher level π^* or possible σ^*_{C-H} assignments. Since there has been some controversy in the past as to the location of the $2\pi^*$ (i.e., levels that correlate with the b_{2g} orbital in benzene) in aromatic species,[9,26,27] these observations provide useful additional information toward the spectroscopic assignments. The spectra of naphthalene, anthracene, and triphenylene are discussed in greater detail below, in comparison to the GSCF3 computational results.

3.4. Comparison with ab Initio Calculations. Figure 3 presents the results of the GSCF3 calculations for C 1s excitation of naphthalene in comparison to the ISEELS result. Table 4 summarizes energies, oscillator strengths, and orbital characters of selected low-energy states from the naphthalene calculation. There are three inequivalent C sites in naphthalene. In addition to showing the site-specific components, Figure 3 compares the predicted total result with the experimental spectra. Note that both energies and intensities are on absolute scale for both the computational and experimental results (energy offsets are used for clarity). The C 1s → π^* features are reproduced reasonably well once the rigid shift between calculation and experiment is made. The agreement between calculation and experiment at higher energies in the core ionization continua is less satisfactory, although there is some correlation with the more intense computed states and the near-threshold broad resonances, which we interpret as being associated with excitations to quasi-bound σ^* states.

It is interesting to compare the present spectral interpretation based on these computations with that previously presented,[14] based on extended Hückel calculations. In that prior work, the theory−experiment comparison suggested that all five virtual π^* levels gave rise to detectible spectral features. The present, more accurate calculations predict that indeed all five levels should produce spectral features. However, some of the computed transitions have zero intensity, resulting in only three of the virtual π^* levels being spectroscopically active for carbon site A, four of them for site B, and all five being active for carbon site C (see Figure 3). A characteristic feature of the naphthalene spectrum, the high-energy shoulder on the first peak (feature 2), is found to arise from excitation to different virtual π^* levels, the $2b_{2g}$ and $2b_{3g}$ levels, as proposed earlier.[14] The intensity pattern that the higher energy peak is of lower intensity than the lower energy peak arises because the C 1s → $2b_{3g}$ transition has zero intensity from carbon site B and low intensity from carbon site C, whereas the C 1s → $2b_{2g}$ transition has high intensity from both carbon sites B and C (although zero intensity from carbon site A). The computed transitions to σ^*-(C−H) and σ^*(C−C) virtual levels occur over a wide energy range (~290−310 eV) with the character gradually changing from σ^*(C−H) to σ^*(C−C) as the transition energy increases. This observation holds for all the molecules studied computationally (Na, An, Tp). The transitions labeled σ^*(C−H)(local) have a final orbital that is virtually pure σ^*(C−H) in character and are heavily localized on the C−H bond attached to the C atom that is computed to contain the core hole. This type of transition is also a feature common to all the molecules studied and occurs in the spectra for all the C atoms that have a H atom attached to them. In addition, this σ^*(C−H)(local)

TABLE 5: Selected Eigenvalues, Oscillator Strengths, and Orbital Characters for Computed Core-Excited States of Anthracene

site	IP	character/ symmetry[a]	orbital	$-\epsilon$ (eV)	$f(10^{-2})$	(R − Å)
A	292.21	π^* $4a_u$	48	−5.202	1.34	2.787
		π^* $5a_u$	49	−3.631	0.68	2.934
		π^* $5b_g$	52	−1.624	0.25	2.888
		π^* $7b_g$	51	0.094	0.61	3.166
		π^* $6a_u$	50	0.679	0.00	2.439
		σ^*(C−H)(local)	82	1.903	1.52	4.529
		π^* $7a_u$	61	3.934	0.51	2.909
		σ^*(C−H & C−C)	54	4.884	0.41	3.388
B	292.12	π^* $4a_u$	48	−5.424	1.29	2.970
		π^* $5a_u$	49	−3.156	0.02	2.923
		π^* $5b_g$	69	−2.235	1.09	2.793
		π^* $7b_g$	50	0.247	0.30	3.160
		π^* $6a_u$	51	0.603	0.00	2.617
		σ^*(C−H)(local)	59	1.758	1.59	3.690
		π^* $7a_u$	52	3.713	0.48	2.944
		σ^*(C−H)	55	4.563	0.13	3.762
		σ^*(C−C)	62	5.082	0.26	3.329
C	292.60	π^* $4a_u$	48	−5.266	0.49	2.655
		π^* $5a_u$	49	−4.276	1.70	2.834
		π^* $5b_g$	50	−2.124	0.38	2.997
		π^* $6a_u$	52	−0.374	0.34	2.635
		π^* $7b_g$	51	0.189	0.05	3.132
		π^* $7a_u$	54	3.340	1.05	3.133
		σ^*(C−H)	56	3.359	0.93	2.832
		σ^*(C−H)	55	4.109	0.33	3.113
		σ^*(C−H & C−C)	61	4.488	0.27	2.660
D	291.850	π^* $4a_u$	48	−5.820	1.15	2.671
		π^* $5a_u$	49	−3.156	0.00	2.828
		π^* $5b_g$	50	−1.566	0.00	3.048
		π^* $6a_u$	52	−0.777	1.03	2.771
		π^* $7b_g$	51	0.285	0.06	3.060
		σ^*(C−H)(local)	66	2.415	1.84	2.732
		π^* $7a_u$	55	3.964	0.00	3.120
		σ^*(C−H)	54	4.806	0.46	3.274
		σ^*(C−H)	53	4.946	0.06	3.491
		σ^*(C−H & C−C)	56	5.340	0.02	2.959

[a] Orbital symmetry in D_{2h}, derived from matching patterns of core-excited symmetry-broken orbitals with correct symmetry, ground-state orbitals. Linear combinations of localized core hole solutions would have these indicated symmetries. The designation "local" for three of the C−H σ^* assignments means that the final orbital density is localized at the C−H bond where the C 1s core hole has been created.

transition has the lowest computed energy of all the σ^* transitions for all molecules studied.

Figure 4 presents the results of the GSCF3 calculations for C 1s excitation of anthracene in comparison to the ISEELS experimental spectrum. Table 5 summarizes energies, oscillator strengths, and orbital character of selected low-energy states from the calculation for anthracene. For anthracene there are four inequivalent C sites, resulting in four calculated spectra. In addition to transitions to different final π^* orbitals, which give rise to several experimentally observed peaks in the 284−288 eV energy loss region, there is doubtless significant peak overlapping and broadening due to transitions to the same final orbital occurring from the different carbon sites. In particular, transitions from carbon site C are predicted to occur at significantly different energies than the equivalent transitions from the three other types of carbon sites. It is also worth noting that due to the different symmetry environments of each type of carbon in anthracene, the intensities of the transitions to the same final π^* orbitals are very different from one another in many cases. Details of the calculated transition energies and intensities can be found in Table 5. These considerations lead to a generally much broader looking π^* spectral region for anthracene than for the other molecules in the present study. The molecule that exhibits the next broadest π^* spectral region is 1,2-benzanthracene, where every carbon site could be considered to be in a slightly different chemical environment, although many of the sites doubtless are very similar to each other. The comments made in the previous section on naphthalene concerning the σ^*(C−H) to σ^*(C−C) transitions apply equally well to the anthracene computational results.

TABLE 6: Selected Eigenvalues, Oscillator Strengths, and Orbital Characters for Computed Core-Excited States of Triphenylene

site	IP	character/ symmetry[a]	orbital	$-\epsilon$ (eV)	$f(10^{-2})$	(R − Å)
A	292.15	π^* $4e''$	62	−4.612	2.03	2.938
		π^* $2a_2''$	124	−3.854	0.00	3.011
		π^* $3a_2''$	61	−2.381	0.08	3.066
		π^* $5e''$	66	−0.763	0.75	3.211
		π^* $6e''$	64	0.596	0.05	2.970
		σ^*(C−H)(local)	71	1.043	0.96	4.752
		π^* $3a_1''$	65	3.263	1.01	3.750
		σ^*(C−H)	126	4.383	0.07	3.766
		σ^*(C−H)	67	4.940	0.08	4.110
		σ^*(C−C)	86	6.947	1.03	3.296
B	292.29	π^* $2a_2''$	65	−4.823	2.04	3.102
		π^* $4e''$	62	−3.938	0.00	2.942
		π^* $3a_2''$	61	−2.48	0.20	3.050
		π^* $5e''$	66	−0.492	0.06	3.218
		π^* $6e''$	64	0.416	0.02	3.201
		σ^*(C−H)(local)	71	0.662	1.11	3.906
		π^* $3a_1''$	82	3.268	0.98	3.134
		σ^*(C−H)	78	4.225	0.05	3.602
		σ^*(C−H & C−C)	84	5.175	0.36	3.627
C	292.53	π^* $4e''$	62	−5.02	1.88	2.963
		π^* $2a_2''$	61	−3.98	0.03	2.934
		π^* $3a_2''$	65	−2.96	0.14	3.103
		π^* $5e''$	66	−0.668	0.02	3.085
		π^* $6e''$	64	0.129	0.05	3.212
		σ^*(C−H)	69	2.672	0.23	3.391
		π^* $3a_1''$	71	2.874	1.05	3.168
		σ^*(C−H)	68	3.878	0.44	3.326
		σ^*(C−H & C−C)	77	4.580	0.77	3.048

[a] Orbital symmetry in D_{2h}, derived from matching patterns of core-excited symmetry-broken orbitals with correct symmetry, ground-state orbitals. Linear combinations of localized core hole solutions would have these indicated symmetries. The designation "local" for two of the C−H σ^* assignments means that the final orbital density is localized at the C−H bond where the C 1s core hole has been created.

Figure 5 presents the results of the GSCF3 calculations for C 1s excitation of triphenylene compared with the ISEELS experimental spectrum. Table 6 summarizes energies, oscillator strengths, and character of selected low-energy states from the calculation for triphenylene. There are three inequivalent C sites in triphenylene. Again, transitions to final orbitals take place at significantly different energies for the different carbon sites; however, they are not spaced widely enough to produce distinct peaks in the experimental spectrum. For triphenylene the most intense π^* feature in the spectrum (lowest energy) is fairly well separated from the other higher energy π^* and Rydberg transitions, and the higher energy π^* peaks are of relatively low intensity. These characteristics result in an overall narrower first π^* peak for triphenylene than for all the other molecules in the present study, except for benzene. Again, the comments made in the earlier section on naphthalene concerning the σ^*-(C−H) to σ^*(C−C) transitions apply equally well to the triphenylene computational results. One additional noteworthy result is that the σ^*(C−H)(local) transitions are predicted by

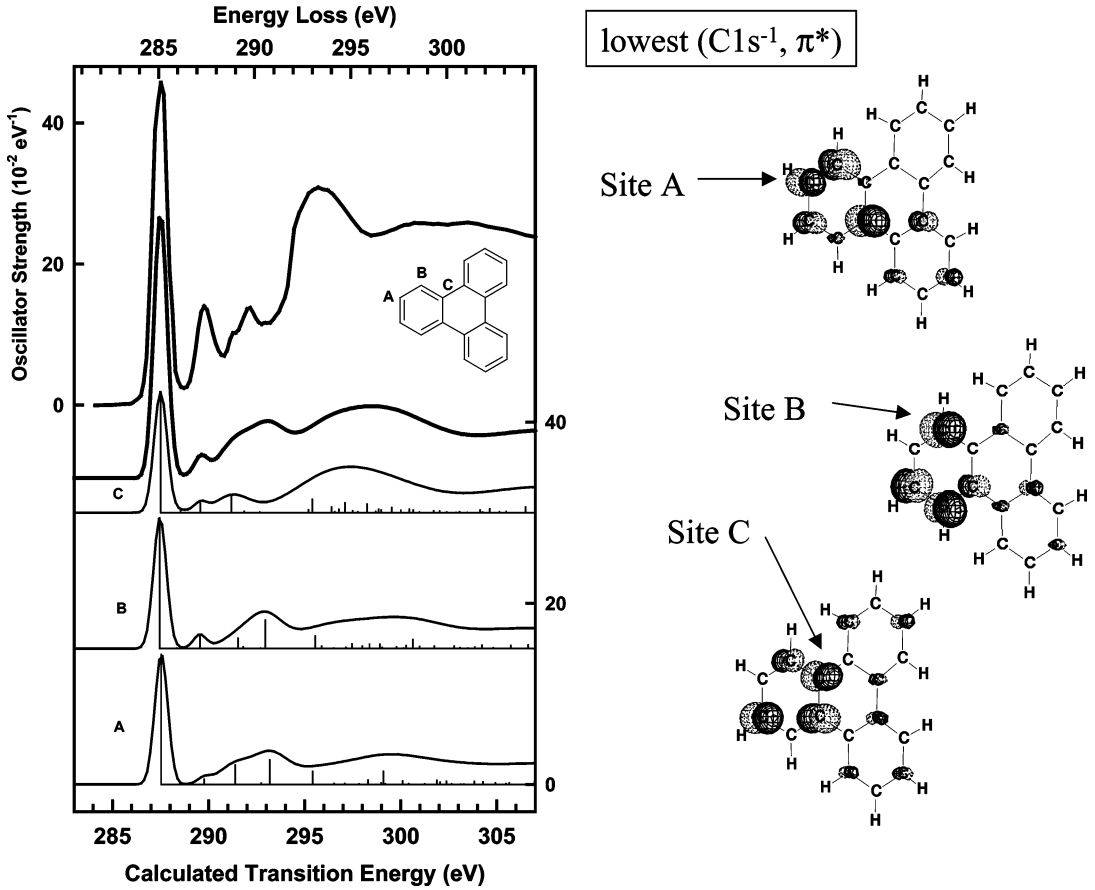

Figure 5. Computed versus measured (ISEELS) spectra of triphenylene. See caption to Figure 3 for further details.

the GSCF3 calculations to occur at significantly lower energies relative to the carbon 1s IPs in triphenylene than for naphthalene or anthracene. This is not simply a function of the size of the molecules, since these transitions are predicted to be at higher energies for anthracene than for naphthalene (see Tables 4−6). Rather, these transitions appear at lower energies in the molecules that exhibit π^* transitions spread over the largest energy.

4. Summary

C 1s electron energy loss spectra of gaseous benzene, naphthalene, anthracene, phenanthracene, triphenylene, pyrene, and 1,2-benzanthracene have been recorded under dipole conditions and assignments proposed for the observed features. Comparison to calculations provides support for the proposed spectral assignments. The XRS of all of these solids except pyrene has been recorded in the C 1s region. Comparison of the spectra by the two techniques indicates the dipole approximation is likely valid for the XRS results; differences between the ISEELS spectrum of gas and the XRS spectrum of solid can be explained by differences in resolution or by quenching of Rydberg transitions in the condensed state.

A number of conclusions might be drawn from these results. On one hand, there is a general trend for species having high symmetry, particularly D_{2h} species such as naphthalene and anthracence, to have significant π^* intensity spread over a larger energy range relative to lower symmetry species such as phenanthracene and 1,2-benzanthracene. A possible explanation is that higher symmetry leads to stronger interactions among states of the same symmetry, in turn leading to a more spread out π^* manifold. The spectral observations could be interpreted alternately to conclude that molecules with a larger number of types of carbon sites show more spread out π^* intensity. To support this view, there is some correlation between the width of the π^* region and the range of C 1s IPs in a molecule. A third perspective is that the more "straight-chain" character the molecule possesses (i.e., benzene rings arranged in a straight line rather than "bent"), the wider the π^* spectral region. At the present time there are not enough data to differentiate among these possible interpretations, but a firm conclusion about the links between molecular structure and nature of the C 1s spectra could lead to useful analytical applications. It is interesting also to note that the ordering of the calculated energies of the σ^*-(C−H)(local) transitions follows the same order as the trend in the π^* transition width; that is, the wider the π^* spectral region, the lower the computed energy of the σ^*(C−H)(local) transitions.

A recent, empirical XRS study[5] of polycyclic aromatic hydrocarbons shows an apparently strong correlation between the width of merged 1s → π^* transitions with the ratio of sextet to double-bond carbons. Cata-condensed (chainlike) systems show a larger 1s → π^* distribution then peri-condensed (circular) ring systems. This observation supports the sextet-double bond description.[29] The detailed theoretical and experimental study shown here will be valuable when using XRS to characterize more complex systems with unknown fused ring composition.

Acknowledgment. This research is supported financially by NSERC (Canada) and the Canada Research Chair program. M.L.G. and D.T. each thank the Department of Chemistry for undergraduate summer research fellowships. This research was partially supported by NIH grants GM-44380 and GM-45440 and NSF grant DMR-0114216 and by the Department of Energy,

Office of Biological and Environmental Research (S.P.C.). The Advanced Photon Source is supported by the Department of Energy, Office of Basic Energy Sciences. BioCAT is a National Institutes of Health-supported Research Center RR-08630.

References and Notes

(1) Clar, E. *Polycyclic Hydrocarbons*; Academic Press: New York, 1964. Chilingarian, G. V.; Yen, T. F. *Bitumens, Asphalts, and Tar Sands*; Elsevier Scientific Pub. Co.; distributors for the U.S. and Canada Elsevier North-Holland: Amsterdam, New York, NY, 1978. Speight, J. G. *The Chemistry and Technology of Petroleum*; M. Dekker: New York, 1980. Mullins, O. C.; Sheu, E. Y. Fine Particle Society Meeting; American Chemical Society, Division of Fuel Chemistry; American Chemical Society, Division of Petroleum Chemistry; *Structures and Dynamics of asphaltenes*; Mullins, O. C., Sheu, E. Y., Eds.; Plenum Press: New York, 1998.

(2) Bergmann, U.; Glatzel, P.; Cramer, S. P. *Microchem. J.* **2002**, *71*, 221.

(3) Bergmann, U.; Cramer, S. P. In *SPIE Conference on Crystal and Multilayer Optics*; SPIE: San Diego, California **1998**, *3448*, 198.

(4) Bergmann, U.; Mullins, O. C.; Cramer, S. P. *Anal. Chem.* **2000**, *72*, 2609.

(5) Bergmann, U.; Groenzin, H.; Mullins, O. C.; Glatzel, P.; Fetzer, J.; Cramer, S. P. *Chem. Phys. Lett.* **2003**, *369*, 184.

(6) Hitchcock, A. P. *J. Electron Spectrosc. Relat. Phenom.* **2000**, *112*, 9.

(7) Hitchcock, A. P. *Phys. Scr.* **1990**, *T31*, 159.

(8) Hitchcock, A. P.; Mancini, D. C. *J. Electron Spectrosc.* **1994**, *67*, 1.

(9) Horsley, J. A.; Stöhr, J.; Hitchcock, A. P.; Newbury, D. C.; Johnson, A. L.; Sette, F. *J. Chem. Phys.* **1985**, *83*, 6099.

(10) Hitchcock, A. P.; Fischer, P.; Gedanken, A.; Robin, M. B. *J. Phys. Chem.* **1987**, *91*, 53.

(11) Ma, Y.; Sette, F.; Meigs, G.; Modesti, S.; Chen, C. T. *Phys. Rev. Lett.* **1989**, *63*, 2044. Ma, Y.; Sette, F.; Meigs, G.; Modesti, S.; Chen, C. T. *Phys. Scr.* **1990**, *41*, 833.

(12) Menzel, D.; Rocker, C.; Steinruck, H. P.; Coulman, D.; Heimann, P. A.; Huber, W.; Zebisch, D.; Lloyd, D. R. *J. Chem. Phys.* **1992**, *96*, 1724.

(13) Kempgens, B.; Köppe, H. M.; Kivimaki, A.; Neeb, M.; Maier, K.; Hergenhahn, U.; Bradshaw, A. M. *Surf. Sci.* **1999**, *425*, L376.

(14) Hitchcock, A. P.; Ishii, I. *J. Electron Spectrosc. Relat. Phenom.* **1987**, *42*, 11.

(15) Sodhi, R. N. S.; Brion, C. E. *J. Electron Spectrosc. Relat. Phenom.* **1984**, *34*, 363.

(16) Mizuno, Y.; Ohmura, Y. *J. Phys. Soc. Jpn.* **1967**, *22*, 445.

(17) Suzuki, T. *J. Phys. Soc. Jpn.* **1967**, *22*, 1139.

(18) Krisch, M. H.; Sette, F.; Masciovecchio, C.; Verbeni, R. *Phys. Rev. Lett.* **1997**, *78*, 2843.

(19) Soininen, J. A.; Hämäläinen, K.; Caliebe, W. A.; Kao, C.-C; Shirley, E. L. *J. Phys.: Condens. Matter* **2001**, *13*, 8039.

(20) Kosugi, N. *Theor. Chim. Acta* **1987**, *72*, 149.

(21) Kosugi, N.; Kuroda, H. *Chem. Phys. Lett.* **1980**, *74*, 490.

(22) Huzinaga, S.; Andzelm, J.; Klobokowski, M.; Radzio-Andzelm, E.; Sasaki, Y.; Tatewaki, H. *Gaussian Basis Sets for Molecular Calculations*; Elsevier: Amsterdam, 1984.

(23) Database of core excitation spectra: http://unicorn.mcmaster.ca/corex.html.

(24) Robin, M. B. *Higher Excited States of Polyatomic Molecules*; Academic Press: New York, 1974−1986; Vols. 1−3.

(25) Steinberger, I. T.; Wassermann, B.; Teodorescu, C. M.; Reichhardt, G.; Gravel, D.; Hutchings, C. W.; Hitchcock, A. P.; Dowben, P. A.; Rühl, E. *Phys. Rev. B* **1999**, *60*, 3995.

(26) Schwarz, W. H. E.; Chang, T. C.; Seeger, U.; Huang, K. H. *Chem. Phys.* **1987**, *117*, 73.

(27) Doering, J. P.; Gedanken, A.; Hitchcock, A. P.; Fischer, P.; Moore, J.; Olthoff, J. K.; Tossell, J.; Raghavachari, K.; Robin, M. B. *J. Am. Chem. Soc.* **1986**, *108*, 3602.

(28) Jolly, W. L.; Bomben, K. D.; Eyermann, C. J. *At. Data Nucl. Data Tables* **1984**, *31*, 433.

(29) Aihara, J. *J. Chem. Phys. A* **1999**, *103*, 7487.

(30) Bruhwiler, P. A.; Maxwell, A. J.; Puglia, C.; Nilsson, A.; Andersson, S.; Martensson, N. *Phys. Rev. Lett.* **1995**, *74*, 614.